Finite Element Method for MRAM Switching Simulations

[1,2]S. FIORENTINI, [1]R. L. DE ORIO, [1,2]J. ENDER, [1]S. SELBERHERR,
[1,2]M. BENDRA, [1,2]N. JØRSTAD, [3]WOLFGANG GOES, [1,2]V. SVERDLOV

[1]Christian Doppler Laboratory for Nonvolatile Magnetoresisitive Memory and Logic at the
[2]Institute for Microelectronics, TU Wien, Gußhausstraße 27–29/E360, 1040 Vienna, AUSTRIA
[3]Silvaco Europe Ltd., Cambridge, UNITED KINGDOM

Abstract: - The development of reliable simulation tools provides a valuable help in the design of modern MRAMdevices. Thanks to its versatility in the choice of meshes and discretization, the finite element method is a useful framework for the numerical solution of the magnetization dynamics. We review a finite element implementation of both the Landau-Lifshitz-Gilbert equation and the spin and charge drift-diffusion formalism in a solver employing open source software. The presented approach is successfully applied to emerging multi-layered MRAM cells.

Keywords: - Finite element method, Landau- Lifshitz-Gilbert equation, spin and charge driftdiffusion, STT-MRAM

Received: March 22, 2022. Revised: November 15, 2022. Accepted: December 13, 2022. Published: December 31, 2022.

1. Introduction

RECENT improvements in the development of complimentary metal-oxide-semiconductor (CMOS) devices have been driven by downscaling of their components. This scaling, however, shows signs of saturation, as it is accompanied by an increase in stand-by power consumption and leakage currents in conventional CMOS technology [1]. The introduction of nonvolatile memory components can help mitigate these issues, as they do not require refreshing of the memory bits. Spin-transfer torque (STT) magnetoresistive random access memory (MRAM) is a viable candidate as a nonvolatile component, thanks to its simple structure and compatibility with CMOS back-end of line processes. It is promising for several stand-alone, embedded automotive and Internet of Things applications, as well as possible employments in frame buffer memory and slow SRAM [2]–[5].

The driving factor of the writing process in modern MRAM cells is the torque generated by the polarization process of electrons transiting through the ferromagnetic layers in a magnetic tunnel junction (MTJ). Development of reliable simulation tools can provide a valuable support for the design of advanced MRAM cells. The simulation of the switching process can be achieved by solving the Landau-Lifshitz-Gilbert (LLG) equation for magnetization dynamics, with the inclusion of a term describing the torque acting on the magnetization. Such term is computed from the non-equilibrium spin accumulation $\mathbf{S}$ in the structure. A solution for $\mathbf{S}$ in all non-magnetic and ferromagnetic layers of an MRAM cell can be obtained by means of the spin and charge drift-diffusion formalism [6]–[8]. Analytical solutions to the drift-diffusion equations, coupled to the LLG, are only possible in simplified scenarios, and numerical methods are necessary to resolve the dynamics in a more general sense. As the finite element (FE) method is naturally able to handle meshes with complex geometries and several material domains [9], [10], in this work we show how it can be employed for the implementation of a solver capable of handling charge, spin accumulation and magnetization dynamics. The implementation was carried out by employing the open-source C++ finite-element library MFEM [11], and can be applied to several MRAM structures.

2. Micromagnetic Equations

The LLG equation for the description of the magnetization dynamics is

$$\frac{\partial \mathbf{m}}{\partial t} = -|\gamma|\mu_0\, \mathbf{m} \times \mathbf{H}_{\text{eff}} + \alpha\, \mathbf{m} \times \frac{\partial \mathbf{m}}{\partial t} + \frac{1}{M_{\text{S}}} \mathbf{T}_{\text{S}}\,. \quad (1)$$

$\mathbf{m} = \mathbf{M}/M_{\text{S}}$ is the unit vector in the direction of the local magnetization, M_{S} is the saturation magnetization, γ is the gyromagnetic ratio, and μ_0 is the vacuum permeability. $\mathbf{H}_{\text{eff}}$ is an effective field including several contributions, like the external field, the exchange coupling, the demagnetizing field and the anisotropy field. $\mathbf{T}_{\text{S}}$ is the spin torque, which can be obtained from the spin accumulation and computed through the spin-charge drift diffusion equations [6], [8]

$$-\boldsymbol{\nabla} \cdot \tilde{\mathbf{J}}_{\text{S}} - D_{\text{e}} \frac{\mathbf{S}}{\lambda_{sf}^2} - \mathbf{T}_{\text{S}} = 0\,, \quad (2a)$$

$$\tilde{\mathbf{J}}_{\text{S}} = -\frac{\mu_B}{e} \beta_\sigma \mathbf{m} \otimes \left(\mathbf{J}_{\text{C}} - \frac{e}{\mu_B} \beta_D D_e (\boldsymbol{\nabla}\mathbf{S})^{\text{T}} \mathbf{m} \right) - D_e \boldsymbol{\nabla}\mathbf{S}\,, \quad (2b)$$

$$\mathbf{T}_{\text{S}} = -D_{\text{e}} \frac{\mathbf{m} \times \mathbf{S}}{\lambda_J^2} - D_{\text{e}} \frac{\mathbf{m} \times (\mathbf{m} \times \mathbf{S})}{\lambda_\varphi^2}\,. \quad (2c)$$

$\tilde{\mathbf{J}}_{\text{S}}$ is the spin current tensor, D_{e} is the electron diffusion coefficient, λ_{sf} is the spin-diffusion length, μ_{B} is the Bohr

magneton, e is the elementary charge, β_σ and β_D are polarization parameters, $\mathbf{J}_\mathrm{C}$ is the charge current density, λ_J is the exchange length and λ_φ is the spin dephasing length.

3. Weak Formulation for a Finite Element Implementation

First schemes for the implementation of a FE algorithm were proposed in [12],[13], by considering only the exchange field contribution to the effective field. In reference [14] the so-called tangent plane integrator scheme, solving for the discrete time derivative, was introduced, and was later generalized to include the full effective field [15], [16]. The unconditional convergence of the tangent plane integrator scheme and of the finite-element implementation of the spin and charge drift-diffusion equations was proven in [17], and later applied to metallic spin-valves in [6]. The weak formulation of the tangent plane integrator and of the spin and charge transport equations are hereby reported.

3.1 LLG Equation

The tangent plane scheme solves the LLG equation for the magnetization derivative $\partial\mathbf{m}/\partial t = \mathbf{v}$. The weak formulation of the standard LLG equation, without the inclusion of the torque term $\mathbf{T}_\mathrm{S}$, comes from the expression

$$\alpha\frac{\partial\mathbf{m}}{\partial t} + \mathbf{m}\times\frac{\partial\mathbf{m}}{\partial t} = |\gamma|\mu_0\,\mathbf{H}_\mathrm{eff} + (\mathbf{m}\cdot\mathbf{H}_\mathrm{eff})\mathbf{m}\,, \qquad (3)$$

which can be obtained by cross-multiplying (1) with $\mathbf{m}$, and using the product rule $\mathbf{a}\times(\mathbf{b}\times\mathbf{c}) = (\mathbf{c}\cdot\mathbf{a})\mathbf{b} - (\mathbf{a}\cdot\mathbf{b})\mathbf{c}$ together with the constraint $|\mathbf{m}| = 1$. For the finite element implementation, the magnetization is taken to be a piecewise affine, globally continuous function [18]. Each component belongs to the Sobolev space H^1. It is the space of functions in L^2 that additionally admit a weak gradient which also belongs to L^2 [16]. The notation for the vector space of the magnetization is $\mathbf{H}^1$. Instead of looking for the solution $\mathbf{v}$ in the same space of the magnetization, the solution space V_T is restricted to vectors tangent to the magnetization, so that $V_\mathrm{T} = \left\{\boldsymbol{w}\in\mathbf{H}^1 \,|\, \mathbf{m}\cdot\boldsymbol{w} = 0\right\}$. The test functions are also restricted to the same space, so that the weak formulation of (3) results in

$$\int_\omega (\alpha\mathbf{v} + \mathbf{m}\times\mathbf{v})\cdot\boldsymbol{w}\,\mathrm{d}\mathbf{x} = |\gamma|\mu_0\int_\omega \mathbf{H}_\mathrm{eff}(\mathbf{m})\cdot\boldsymbol{w}\,\mathrm{d}\mathbf{x}\,. \qquad (4)$$

ω is the subdomain containing only the magnetic parts of the structure under analysis. The last term on the right-hand side of (3) is not present, as the test functions are restricted to the tangent space V_T. The time derivative $\mathbf{v}$ at a certain time t^k is obtained by setting [18]

$$\mathbf{m}^{\mathrm{k}+1} = \mathbf{m}^\mathrm{k} + \theta\delta t\mathbf{v}\,. \qquad (5)$$

δt is the time-step, and θ is a parameter between 0 and 1, with the value 0 leading to a fully explicit scheme and 1 to a fully implicit one. Each effective field contribution can be treated with a different value of θ. In the implementation employed for this work, θ is different from 0 only for the exchange field contribution, were the value 1 is employed for stability reasons [19]. The weak formulation employed for the computation of the magnetization dynamics by the FE solver is then, with the inclusion of the torque terms coming from (2):

$$\int_\omega (\alpha\mathbf{v} + \mathbf{m}^\mathrm{k}\times\mathbf{v})\cdot\boldsymbol{w}\,\mathrm{d}\mathbf{x} + \frac{2A|\gamma|}{M_S}\delta t\int_\omega \boldsymbol{\nabla}\mathbf{v} : \boldsymbol{\nabla}\boldsymbol{w}\,\mathrm{d}x = -\frac{2A|\gamma|}{M_S}\int_\omega \boldsymbol{\nabla}\mathbf{m}^\mathrm{k} : \boldsymbol{\nabla}\boldsymbol{w}\,\mathrm{d}\mathbf{x} + \gamma_0\int_\omega \mathbf{H}_\mathrm{eff}\cdot\boldsymbol{w}\,\mathrm{d}x + \frac{D_\mathrm{e}}{M_\mathrm{S}}\int_\omega\left(\frac{\mathbf{S}^\mathrm{k}}{\lambda_J^2} + \frac{\mathbf{m}^\mathrm{k}\times\mathbf{S}^\mathrm{k}}{\lambda_\varphi^2}\right)\cdot\boldsymbol{w}\,\mathrm{d}\mathbf{x} \qquad (6a)$$

$$\mathbf{m}^{\mathrm{k}+1} = \frac{\mathbf{m}^\mathrm{k} + \delta t\,\mathbf{v}}{|\mathbf{m}^\mathrm{k} + \delta t\,\mathbf{v}|} \qquad (6b)$$

The right-hand side of (6b) is evaluated nodewise, and $\boldsymbol{\nabla}\mathbf{a} : \boldsymbol{\nabla}\mathbf{b} = \sum_{\mathrm{ij}}(\partial a_\mathrm{i}/\partial x_\mathrm{j})(\partial b_\mathrm{i}/\partial x_\mathrm{j})$ is the Frobenius inner product of two matrices. The exchange field contribution, together with (5), gives rise to the second term on the left-hand side and to the first term on the right-hand side. The boundary integrals arising from the weak formulation of this contribution are put to zero by the Neumann boundary condition $(\boldsymbol{\nabla}\mathbf{m})\mathbf{n} = \mathbf{0}$ (with $\mathbf{n}$ the boundary normal), applied on the external boundary of the magnetic region $\partial\omega$. $\mathbf{H}_\mathrm{eff}$ contains the remaining effective field contributions. The equations are subject to the initial condition $\mathbf{m}(0) = \mathbf{m}^0$. The system of equations resulting from the FE implementation of this weak formulation includes the tangent plane constraint $\mathbf{m}\cdot\boldsymbol{w} = 0$, and the solution at each time-step is computed through a solver based on the generalized minimal residual (GMRES) method, provided by the library MFEM. The GMRES method is designed for indefinite non-symmetric systems of linear equations, as is the case of FE implementation of (6a) due to the presence of the cross-product terms. Material parameters that can differ from subdomain to subdomain are treated as piecewise constant functions, unless differently stated. The contribution of the demagnetizing field is evaluated only on the disconnected magnetic domain by using a hybrid approach combining the boundary element method and the FE method [20], [21].

3.2 Spin and Charge Drift-Diffusion Equations

The weak formulation for the computation of the spin accumulation is derived from (2). The equations are solved for the magnetization $\mathbf{m}^\mathrm{k}$ at each time-step, and the resulting spin accumulation $\mathbf{S}^\mathrm{k}$ is employed in (6a).

For the computation of the charge potential and current, a Laplace equation is solved for the whole domain Ω, with the weak formulation

$$\int_\Omega \sigma \boldsymbol{\nabla} V \cdot \boldsymbol{\nabla} v \, \mathrm{d}\mathbf{x} = 0 \,, \tag{7a}$$

$$\int_\Omega \mathbf{J}_\mathrm{C} \cdot \boldsymbol{v} \, \mathrm{d}\mathbf{x} = -\int_\Omega \sigma \boldsymbol{\nabla} V \cdot \boldsymbol{v} \, \mathrm{d}\mathbf{x} \,. \tag{7b}$$

v represents a test function belonging to H^1, while $\boldsymbol{v}$ is a test function in $\mathbf{H}^1$. V belongs to H^1, and equation (7b) is employed to obtain a projection of $\mathbf{J}_\mathrm{C}$ in the $\mathbf{H}^1$ function space [18]. Dirichlet conditions are applied to prescribe the voltage at the contacts. The Neumann condition $\sigma \boldsymbol{\nabla} V \cdot \mathbf{n} = 0$ is assumed on external boundaries not containing an electrode. Special treatment of the conductivity σ results in an implementation capable of reproducing the charge current dependence on the tunnel magnetoresistance (TMR) and relative direction of the magnetization vectors in the free layer (FL) and reference layer (RL) of an MTJ [22]. The solution of the system of equations resulting from the FE implementation of (7) is computed through a solver based on the conjugate gradient (CG) method, provided by the library MFEM. The CG method is designed for the numerical solution of systems of linear equations whose matrix is positive-definite, as is the case of the FE implementation of (7).

The weak formulation of the spin drift-diffusion equations presented in [6] was generalized to apply to (2) which includes the additional spin dephasing term, resulting in the following expression:

$$\begin{aligned} &D_\mathrm{e} \int_\Omega \left(\boldsymbol{\nabla} \mathbf{S} - \beta_\sigma \beta_\mathrm{D} \mathbf{m} \otimes \left((\boldsymbol{\nabla} \mathbf{S})^\mathrm{T} \mathbf{m} \right) \right) : \boldsymbol{\nabla} \boldsymbol{v} \, \mathrm{d}\mathbf{x} + \\ &+ D_\mathrm{e} \int_\Omega \left(\frac{\mathbf{S}}{\lambda_{sf}^2} + \frac{\mathbf{S} \times \mathbf{m}}{\lambda_J^2} + \frac{\mathbf{m} \times (\mathbf{S} \times \mathbf{m})}{\lambda_\varphi^2} \right) \cdot \boldsymbol{v} \, \mathrm{d}\mathbf{x} = \\ &\frac{\mu_B}{e} \beta_\sigma \int_\omega (\mathbf{m} \otimes \mathbf{J}_\mathrm{C}) : \boldsymbol{\nabla} \boldsymbol{v} \, \mathrm{d}\mathbf{x} + \\ &- \frac{\mu_B}{e} \beta_\sigma \int_{\partial\Omega \cap \partial\omega} ((\mathbf{m} \otimes \mathbf{J}_\mathrm{C}) \mathbf{n}) \cdot \boldsymbol{v} \, \mathrm{d}\mathbf{x} \,. \end{aligned} \tag{8}$$

$\boldsymbol{v}$ represents again a test function belonging to $\mathbf{H}^1$, $\mathbf{S}$ also belongs to $\mathbf{H}^1$, and $\partial\Omega \cap \partial\omega$ indicates the shared external boundary of the whole domain Ω and magnetic subdomain ω. The boundary integrals arising from the weak formulation are put to zero by the Neumann condition $(\boldsymbol{\nabla} \mathbf{S})\mathbf{n} = \mathbf{0}$, assumed on external boundaries. For contacting regions longer than the spin-flip length, this condition is equivalent to an exponential decay of $\mathbf{S}$ towards the electrodes [6], [8]. The charge current $\mathbf{J}_\mathrm{C}$ is the one computed from (7). The addition of appropriate boundary conditions at the interfaces between the tunnel barrier and the RL and FL allows to reproduce the torque properties typical of MTJs [23]. The solution of the system of equations resulting from the FE implementation of (8) is computed through a solver based on the GMRES method, provided by the library MFEM, as due to the cross product terms the FE implementation of (8) results in a non-symmetric system of linear equations.

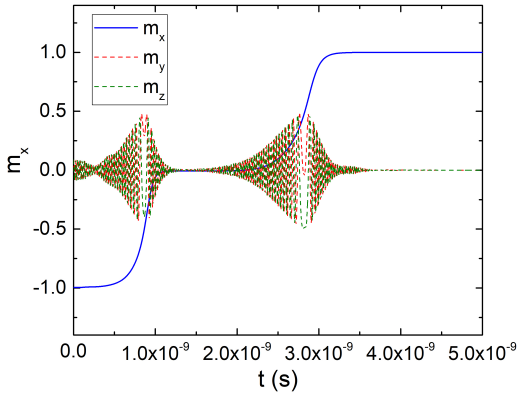

Fig. 1: Anti-parallel to parallel switching of elongated MRAM cell with composite FL. The two FL segments switch one at a time, creating visible steps in the switching process.

4. Applications

The solver implementing the proposed approach can be applied to various structures composed of ferromagnets, metal spacers, and tunnel barriers. It is particularly suitable for simulating recently proposed devices presenting additional layers for the reduction of switching current and cell size. Application of the solver to elongated structures with composite FL, proposed in [24], reveals a step-by-step switching process [23], and allows to evaluate the possibility of using such structures as multi-bit cells. The anti-parallel to parallel switching of a structure with two FL segments is reported in Fig.1. The solver was also successfully applied to the switching simulation of structure presenting a double FL [25], reproducing the observed reduction of the switching voltage [26]. Additional terms in the spin current expression allow to also reproduce the spin Hall effect [8], so that the solver can also be applied to switching simulations of spin-orbit torque (SOT) MRAM [27].

5. Conclusion

We presented a finite element implementation of the weak formulation of the LLG equation coupled to spin transport in a solver based on open source software. The developed solver has been successfully applied to switching simulations of emerging experimental structures composed of multiple ferromagnetic layers, nonmagnetic spacers and tunnel barriers, and can be a valuable help to predict and investigate the switching behavior of novel structures.

Acknowledgment

The financial support by the Austrian Federal Ministry for Digital and Economic Affairs and the National Foundation for Research, Technology and Development is gratefully acknowledged.

References

[1] T. Hanyu, T. Endoh, D. Suzuki, H. Koike, Y. Ma *et al.*, "Standby-power-free integrated circuits using MTJ-based VLSI computing," Proc. IEEE, vol. 104, no. 10, pp. 1844–1863, 2016.

[2] W. J. Gallagher, E. Chien, T. Chiang, J. Huang, M. Shih *et al.*, "22nm STT-MRAM for reflow and automotive uses with high yield, reliability, and magnetic immunity and with performance and shielding options," in Proc. IEDM Conf., 2019, pp. 2.7.1–2.7.4.

[3] S. H. Han, J. M. Lee, H. M. Shin, J. H. Lee, K. S. Suh *et al.*, "28nm 0.08 mm^2/Mb embedded MRAM for frame buffer memory," in Proc. IEDM Conf., 2020, pp. 11.2.1–11.2.4.

[4] Y.-C. Shih, C.-F. Lee, Y.-A. Chang, P.-H. Lee, H.-J. Lin *et al.*, "A reflow-capable, embedded 8Mb STT-MRAM macro with 9ns read access time in 16nm FinFET logic CMOS process," in Proc. IEDM Conf., 2020, pp. 11.4.1–11.4.4.

[5] V. B. Naik, K. Yamane, T. Lee, J. Kwon, R. Chao *et al.*, "JEDEC-qualified highly reliable 22nm FD-SOI embedded MRAM for low-power industrial-grade, and extended performance towards automotive-grade-1 applications," in Proc. IEDM Conf., 2020, pp. 11.3.1–11.3.4.

[6] C. Abert, M. Ruggeri, F. Bruckner, C. Vogler, G. Hrkac *et al.*, "A three-dimensional spin-diffusion model for micromagnetics," Sci. Rep., vol. 5, no. 1, p. 14855, 2015.

[7] C. Abert, M. Ruggeri, F. Bruckner, C. Vogler, A. Manchon *et al.*, "A self-consistent spin-diffusion model for micromagnetics," Sci. Rep., vol. 6, no. 1, p. 16, Dec. 2016.

[8] S. Lepadatu, "Unified treatment of spin torques using a coupled magnetisation dynamics and three-dimensional spin current solver," Sci. Rep., vol. 7, no. 1, p. 12937, 2017.

[9] D. Braess, Finite Elements: Theory, Fast Solvers, and Applications in Solid Mechanics, 3rd ed. Cambridge University Press, 2007.

[10] M. G. Larson and F. Bengzon, The Finite Element Method: Theory, Implementation, and Applications. Springer Berlin Heidelberg, 2013.

[11] R. Anderson, J. Andrej, A. Barker, J. Bramwell, J.-S. Camier *et al.*, "MFEM: A modular finite element library," Comp. & Math. with Appl., 2020.

[12] F. Alouges and P. Jaisson, "Convergence of a finite element discretization for the Landau-Lifshitz equations in micromagnetism," Math. Models Methods Appl. Sci., vol. 16, no. 2, p. 299 – 316, 2006.

[13] S. Bartels, J. Ko, and A. Prohl, "Numerical analysis of an explicit approximation scheme for the Landau-Lifshitz-Gilbert equation," Math. Comput., vol. 77, no. 262, p. 773 – 788, 2008.

[14] F. Alouges, "A new finite element scheme for Landau-Lifchitz equations," Discrete Contin. Dyn. Syst. S, vol. 1, no. 2, pp. 187–196, 2008.

[15] F. Alouges, E. Kritsikis, and J.-C. Toussaint, "A convergent finite element approximation for Landau–Lifschitz–Gilbert equation," Physica B, vol. 407, no. 9, pp. 1345–1349, 2012.

[16] F. Bruckner, D. Suess, M. Feischl, T. Führer, P. Goldenits *et al.*, "Multiscale modeling in micromagnetics: Existence of solutions and numerical integration," Math. Models Methods Appl. Sci., vol. 24, no. 13, pp. 2627–2662, 2014.

[17] C. Abert, G. Hrkac, M. Page, D. Praetorius, M. Ruggeri, and D. Suess, "Spin-polarized transport in ferromagnetic multilayers: An unconditionally convergent FEM integrator," Comp. & Math. with Appl., vol. 68, no. 6, pp. 639 – 654, 2014.

[18] C. Abert, "Micromagnetics and spintronics: Models and numerical methods," Eur. Phys. J. B, vol. 92, no. 6, p. 120, June 2019.

[19] G. Hrkac, C.-M. Pfeiler, D. Praetorius, M. Ruggeri, A. Segatti, and B. Stiftner, "Convergent tangent plane integrators for the simulation of chiral magnetic skyrmion dynamics," Adv. Comput. Math., vol. 45, no. 3, pp. 1329–1368, June 2019.

[20] J. Ender, M. Mohamedou, S. Fiorentini, R. L. de Orio, S. Selberherr *et al.*, "Efficient demagnetizing field calculation for disconnected complex geometries in STT-MRAM cells," in Proc. SISPAD Conf., 2020, pp. 213–216.

[21] M. Bendra, J. Ender, S. Fiorentini, T. Hadamek, R. L. de Orio *et al.*, "Finite element method approach to MRAM modeling," in Proc. MIPRO Conf., 2021, pp. 70–73.

[22] S. Fiorentini, J. Ender, S. Selberherr, R. L. de Orio, W. Goes, and V. Sverdlov, "Coupled spin and charge drift-diffusion approach applied to magnetic tunnel junctions," Solid-State Electron., vol. 186, p. 108103, 2021.

[23] S. Fiorentini, M. Bendra, J. Ender, R. L. de Orio, W. Goes *et al.*, "Spin and charge drift-diffusion in ultra-scaled MRAM cells," Sci. Rep., vol. 12, no. 1, p. 20958, Dec. 2022.

[24] B. Jinnai, J. Igarashi, K. Watanabe, T. Funatsu, H. Sato *et al.*, "High-performance shape-anisotropy magnetic tunnel junctions down to 2.3 nm," in Proc. IEDM Conf., 2020, pp. 24.6.1–24.6.4.

[25] G. Hu, G. Lauer, J. Z. Sun, P. Hashemi, C. Safranski *et al.*, "2X reduction of STT-MRAM switching current using double spin-torque magnetic tunnel junction," in Proc. IEDM Conf., 2021, pp. 2.5.1–2.5.4.

[26] W. J. Loch, S. Fiorentini, N. P. Jørstad, W. Goes, S. Selberherr, and V. Sverdlov, "Double reference layer STT-MRAM structures with improved performance," Solid-State Electron., vol. 194, p. 108335, 2022.

[27] N. P. Jørstad, S. Fiorentini, W. J. Loch, W. Goes, S. Selberherr, and V. Sverdlov, "Finite element modeling of spin–orbit torques," Solid-State Electron., vol. 194, p. 108323, 2022.